Microscopic Observations and Simulations of Bloch Walls in Nematic Thin Films

Jian Zhou,[1] Jung O. Park,[1,2] Gino De Luca,[3] Alejandro D. Rey,[3] and Mohan Srinivasarao[1,2,4]

[1]*School of Polymer, Textile and Fiber Engineering, Georgia Institute of Technology, Atlanta, Georgia 30332, USA*
[2]*Center for Advanced Research on Optical Microscopy (CAROM), Georgia Institute of Technology, Atlanta, Georgia 30332, USA*
[3]*Department of Chemical Engineering, McGill University, Montreal, Quebec H3A 2B2, Canada*
[4]*School of Chemistry and Biochemistry, Georgia Institute of Technology, Atlanta, Georgia 30332, USA*

(Received 7 March 2006; published 11 October 2006)

We study Bloch wall defects formed by quenching nematic thin films from planar anchoring to homeotropic anchoring through a temperature-driven anchoring transition. The director profiles of the walls are directly visualized using fluorescence confocal polarizing microscopy, and shown to agree well with the simulation based on the Frank elasticity theory. A pure twist wall exists if the ratio of sample thickness to surface extrapolation length p is smaller than or close to 1; while a diffuse Bloch wall is obtained if p is much greater than 1.

DOI: 10.1103/PhysRevLett.97.157801 PACS numbers: 61.30.−v

A nematic liquid crystal (LC) possesses long range orientational order along a direction $\boldsymbol{n}$, known as the director. A wall defect in a nematic phase is a two-dimensional defect that separates regions with different director orientation, which usually forms during a fast realignment process. One such example is the Freedericksz transition, where the LC director is realigned by an external field perpendicular to the original alignment [1]. The director can rotate in two opposite directions [$\boldsymbol{n} = -\boldsymbol{n}$] in response to the applied field, thus leading to a 180° inversion wall [1,2]. Figure 1(a) shows a schematic director configuration of the so-called Bloch wall [3] consisting of 180° twist deformation along the x direction. In this figure, d is the Bloch wall thickness and h is the sample thickness. Helfrich first theoretically described the director configuration of inversion walls formed due to the application of a magnetic field [4]. Such wall defects are usually unstable and collapse on themselves in a short time, but can be stabilized by the bounding surfaces. Ryschenkow and Kleman first reported that Bloch walls were formed in nematic thin films due to temperature-driven anchoring transitions and remained stable due to weak homeotropic or tilted anchoring [5]. They proposed that the polar anchoring strength (W_p) can be estimated from the geometry of the wall: $W_p \sim K_{22}h/d^2$, where K_{22} is the twist elastic constant of the nematics. They predicted and experimentally demonstrated that when the surface extrapolation length b (defined as K_{22}/W_p) is $\geq h$, a pure twist wall is obtained, while a diffuse Bloch wall is obtained when $b \ll h$. In practice, the wall thickness d, instead of b, may be compared with h to judge which regime the wall belongs to, because d is easily obtained from a microscopic observation. However, we know of no instance where such a diffuse Bloch wall has been clearly demonstrated in experimental observations.

With the help of fluorescence confocal polarizing microscopy (FCPM), one is able to observe three-dimensional nematic director configuration [6–8]. In the first part of this Letter, we show direct visualization of two types of Bloch walls, pure twist walls and diffuse walls, using FCPM technique. This is followed by a simulation of the evolution of the Bloch walls with varying anchoring strengths using Frank elasticity. These simulations agree remarkably well with the experimental FCPM observation.

Nematic fluids we used were TL205 (birefringence $\Delta n = 0.22$) and MLC6608 ($\Delta n = 0.083$) from EMerck

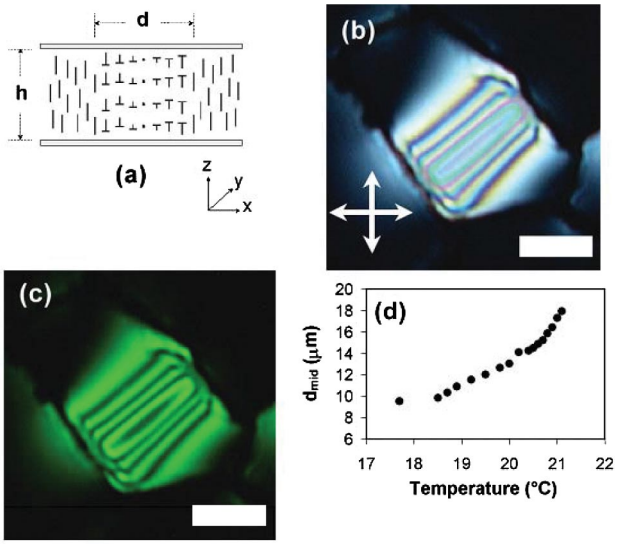

FIG. 1 (color). (a): A pure twist Bloch wall with the wall thickness d (parallel to x), in a nematic film of thickness h (parallel to z). The head of the nail sign, "T", represents the end of the nematic director below the paper plane. (b) and (c): Microscope images (under crossed polarizers and at 45° to the incident polarization) of a Bloch wall in a film of TL205 ($h = 15$ μm) in the xy plane with (b) white light and (c) monochromatic (532 nm) illumination. The scale represents 10 μm. (d): Wall thickness d_{mid} at $z = 0$ as a function of temperature near the homeotropic-to-planar anchoring transition ($T_t = 21$ °C).

Industries. Acrylate monomers, *n*-octyl acrylate, isobonyl acrylate, isooctyl acrylate, and 1,1,1-trimethylol propane triacrylate (Scientific Polymer Products) were used without further purification. The amount of triacrylate was about 10 wt% of the total monomer, which provides the rigidity of LC-polymer composite films through cross-linking reaction. The films were prepared by photopolymerization-induced phase separation reported previously [9]. Such films contain polygonal LC domains of 30–50 μm in width. The film thickness was controlled by glass microbeads of standard size (Duke Scientific, 5 and 15 μm in diameter). Bloch walls were formed by quenching a film with a planar alignment from relatively high temperature to homeotropic alignment through a temperature-driven transition [8–11].

About 0.003 wt% of a fluorescent dye, pyrromethene 546 (Exciton), was also added to the prepolymerization mixtures to help the characterization of the director field using FCPM. The fluorescence transition dipole of the dye was found to align parallel to the local nematic director [7]. The intensity of the fluorescence is maximum when the polarization of the excitation beam, **E**, is parallel to $\boldsymbol{n}$, and minimum when **E** is perpendicular to $\boldsymbol{n}$, with the ratio of 2.2. The dye was excited using an Ar^+ laser at 488 nm and the fluorescence was collected at 520–560 nm.

A Bloch wall in a composite film of TL205 and poly(isooctyl acrylate) between crossed polars, shows symmetric and parallel color bands with respect to the center *yz* plane of the wall [Fig. 1(b)] when a white light source is used. The color sequence from either edge of the wall to the central plane follows that of the Michel-Levy birefringence chart [5,12]. In monochromatic light, the wall between crossed polarizers shows interference fringes parallel to the wall [Fig. 1(c)]. When the wall is perpendicular (parallel) to the polarizer, it shows no (best) imaging contrast on removal of the analyzer. This is because the largest variation in refractive index is obtained when the polarization of light is parallel to the wall. A structure with such a refractive index variation functions as a lens [13] and generates a thin bright line. All of the above observations confirm that the defect is a Bloch wall.

In addition, when the films with Bloch walls are heated close to the homeotropic-to-planar anchoring transition temperature (T_t), the thickness of wall d continuously expands [Fig. 1(d)], indicating a decrease in the anchoring strength near T_t.

We choose the low birefringence MLC6608 LC to avoid or minimize optical aberrations in confocal imaging [7,11,14] and Bloch walls in MLC6608 + poly(isooctyl acrylate) were imaged using FCPM. By controlling the film thickness relative to the width of the wall, the two types of Bloch walls proposed by Ryschenkow and Kleman were realized, Fig. 2.

Figure 2(a) presents the *xy* and *xz* optical sections of a pure twist Bloch wall in a 8 μm thick film. The fluorescence emission of the dye is proportional to its absorbance, which in turn depends on the average orientation of the absorption dipoles of the dye molecules with respect to the polarization of the excitation **E**. Since the absorption dipole of the dye is parallel to the local LC director, the measured fluorescence intensity provides us information on the director orientation. The spatial orientation of a nematic director can be specified by two angles: tilt angle θ ($\theta = 0$ along the substrate normal direction), and azimuthal angle ϕ ($\phi = 0$ along the orientation of the wall projection in *xy* plane). Since the azimuthzal angle of the director within a Bloch wall is zero, the angle between the director (or the absorption dipole of the dye) and **E** equals $\pi/2$-θ in Fig. 2. This simplified relation between the fluorescence intensity of the dye and the orientation of the director, $\boldsymbol{n}(\theta)$ is described by [15] $I_{\text{fluor}}(\theta) \propto I_{\text{em}}(\theta) \propto A(\theta) \propto \sin^2(\theta)$, where I_{fluor} is the fluorescence intensity collected by the detector, I_{em} is the emission intensity of the dye, and A is the dye absorbance.

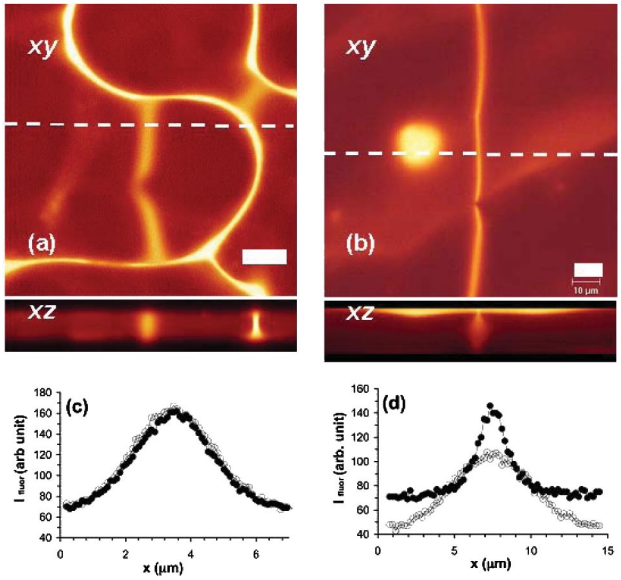

FIG. 2 (color). Confocal fluorescence images (*xy* and *xz* sections) of two Bloch walls: (a) with the extrapolation length (ca. 4.5 μm) $\sim$ the sample thickness (8.0 μm); and (b) with the extrapolation length $\ll$ the sample thickness (18 μm). The *xz* section is along the dashed line shown in the *xy* section and located 1 μm below the top LC-polymer interface. (c): The fluorescence intensity profiles across the wall in (a) at a depth of 1 μm (●) and 4 μm (○), respectively, below the top interface. (d): The fluorescence intensity profiles across the wall in (b) were taken at 1 μm (●) and 5 μm (○) below the top interface. The excitation polarization in (a) and (b) is along *y* axis. The scale bars shown in (a) and (b) represent 10 μm.

As shown in Fig. 2(c), the profiles of the fluorescence intensity across the wall at different depths of the film (open and closed circles) almost overlap with each other, which suggests that the director variation along *z* axis, $\partial\theta/\partial z$, is negligible [5]. The wall therefore contains only

a twist deformation; i.e., it is a pure twist wall. Here the wall thickness d (ca. 6 μm) is comparable with the thickness h (8 μm).

Figure 2(b) shows the confocal images of a Bloch wall in a 18 μm-thick film which was made from the same film recipe as Fig. 2(a). However, d is a function of z, smallest near both top and bottom substrates, and largest at the middle depth of the film, i.e., showing a barrel-like profile in the xz optical section. The difference between the fluorescence intensity profiles across the wall at different depths [Fig. 2(d)] suggests that $\partial\theta/\partial z \neq 0$. In this case, d near either of the substrate is much smaller than h. Therefore, our result is consistent with Kleman's prediction: a diffuse wall is more stable when the surface extrapolation length b is much smaller than the thickness h.

We now proceed to the simulations of our experiments based on Frank elasticity of the nematic fluid which is expressed as $F = \int_v f_b dv + \int_s f_s ds$.

According to Frank's formalism, the bulk elastic free energy density, in the one constant approximation, can be written as [1] $f_b = \frac{k}{2}(\nabla \boldsymbol{n})\colon(\nabla \boldsymbol{n})^T$, where k is a material-dependent elastic constant. The surface free energy density can be derived from Rapini-Papoular expression and reads: $f_s = \frac{w}{2}[1 - (\boldsymbol{n}\cdot\boldsymbol{e})^2]$ [16], where w is the surface anchoring strength and $\boldsymbol{e}$ a unit vector giving some preferred orientation of the nematic director at the surface also called easy axis. Any deviation of the director $\boldsymbol{n}$ from $\boldsymbol{e}$ leads to a free energy penalty proportional to w.

A key length scale for this problem is b which is defined as the ratio of bulk to surface energy densities $b = k/w$. According to the continuum theory, the thermodynamically stable states of a system are the ones characterized by free energy minima [17]. In order to study the effect w on the equilibrium structure of Bloch walls, we therefore need to seek director fields that minimize the total free energy. The equations governing this problem are derived using variational calculus [18].

The computational domain considered is a simple 2D slice taken along the thickness of the nematic thin film in the x-z plane. The Euler-Lagrange equation associated with the variational problem is [1]

$$\frac{\partial f_b}{\partial \boldsymbol{n}} - \nabla\cdot\frac{\partial f_b}{\partial \nabla \boldsymbol{n}} = \lambda_b \boldsymbol{n}$$

where λ_b is a Lagrange multiplier introduced to fulfill the unit length constraint of $\boldsymbol{n}$. This equation is numerically solved subject to general boundary conditions:

$$\frac{\partial f_s}{\partial \boldsymbol{n}} + \boldsymbol{\nu}\cdot\frac{\partial f_s}{\partial \nabla \boldsymbol{n}} = \lambda_s \boldsymbol{n}, \tag{1}$$

where $\boldsymbol{\nu}$ is the outward unit normal to the surface and λ_s is the surface Lagrange multiplier [18,19]. In order to facilitate the analysis of the simulation results, the set of equations are nondimensionalized. The reference length scale in this problem is the thickness of the film and therefore we define the dimensionless position vector as $\bar{\mathbf{r}} = r/h$. The key parameter in this problem then becomes the dimensionless surface anchoring strength defined as $p = h/b = (hw)/k$.

The boundaries conditions on the sides of the computational domain are considered to be of the Neumann type to emulate an infinitely wide sample and remove or neglect

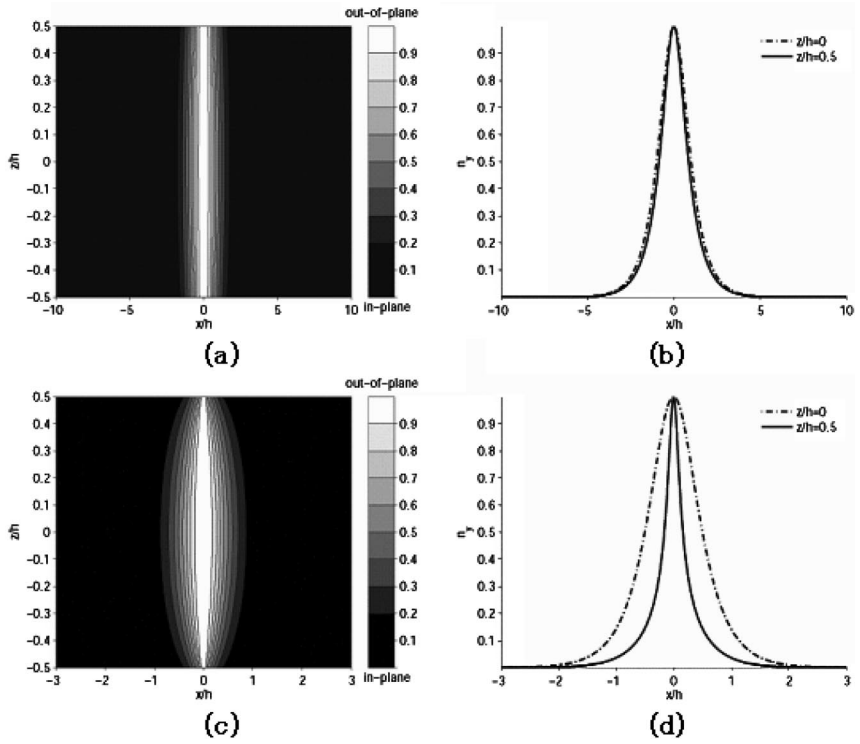

FIG. 3. (a) Surface plot of the component n_y, when the dimensionless surface anchoring strength p is equal to 1. The director field is nearly uniform throughout the sample thickness. (b) Profiles of n_y at the surface ($z/h = 0.5$) and midplane ($z/h = 0$) when $p = 1$. (c) and (d) same type of plots for the case of $p = 10$ under a strong anchoring.

any lateral surface torques. On the upper and lower surfaces, Eq. (1) is solved with different dimensionless surface anchoring strengths and an easy direction normal to the surfaces.

We examine the structure of an 180° twist wall when the dimensionless surface anchoring strength is $p = 1$. Figure 3(a) shows that for this value of p, the director orientation in the wall is almost independent of the nematic film thickness. The structure of this quasi-pure Bloch wall is more easily seen from Fig. 3(b), which shows the profiles of n_y, at surface and middle depth of the sample. The profiles of n_y found in Fig. 3(b) agree very well with the fluorescence intensity profiles obtained experimentally [Fig. 2(c)], where the surface anchoring strength was close to 1.

Figures 3(c) and 3(d) present director configurations obtained for $p = 10$, i.e., strong anchoring. Figure 3(c) illustrates that, as the deviation from the easy axis becomes more costly, the wall deforms in a barrel-like fashion. The wall is clearly wider at middle depth than at surfaces and is referred as diffuse. Figure 3(d) presents two profiles of n_y through the thickness of the film illustrating the net variations of the wall width. Results in Fig. 3(d) are consistent with the fluorescence intensity profile shown in Fig. 2(d). In the case of $p < 1$, the simulation reveals that there are no variations of the director orientation through the thickness of the nematic film. The 180° twist wall is accordingly a pure Bloch wall and the profiles of the n_y component at the top surface and the middle plane perfectly coincide as no variations of θ occur. The Bloch wall thickness was much larger than that of the case of $p = 1$, confirming its increase with the anchoring strength decrease.

In summary, we have shown using FCPM and numerical simulation that when $d \sim h$, a pure twist wall results and when $d < h$, a diffuse wall with a barrel-like profile results. This behavior can be easily understood by looking at the free energy expressions at the surface and in the bulk. The surface energy is minimized as the thickness of the wall becomes smaller, while the bulk elastic energy decreases with decreasing gradients of the director orientations and therefore extends the thickness of the wall. These conflicting mechanisms for the minimization of the system free energy leads to the diffuse Bloch wall structure experimentally observed.

This work was supported by a National Science Foundation Grant No. DMR-0312792. Gino De Luca acknowledges support from the Department of Chemical Engineering of McGill University.

[1] P. G. de Gennes and J. Prost, *The Physics of Liquid Crystals* (Clarendon, Oxford, 1993).
[2] L. Leger, Mol. Cryst. Liq. Cryst. **24**, 33 (1973).
[3] M. Kleman, *Points, Lines and Walls* (John Wiley & Sons, New York, 1983).
[4] W. Helfrich, Phys. Rev. Lett. **21**, 1518 (1968).
[5] G. Ryschenkow and M. Kleman, J. Chem. Phys. **64**, 404 (1976).
[6] D. Voloschenko and O. D. Lavrentovich, Opt. Lett. **25**, 317 (2000).
[7] I. I. Smalyukh, S. V. Shiyanovskii, and O. D. Lavrentovich, Chem. Phys. Lett. **336**, 88 (2001).
[8] J. Zhou, Ph.D. thesis, Georgia Institute of Technology, 2004.
[9] J. Zhou *et al.*, J. Am. Chem. Soc. **124**, 9980 (2002).
[10] K. R. Amundson and M. Srinivasarao, Phys. Rev. E **58**, R1211 (1998).
[11] J. Zhou *et al.*, J. Phys. Chem. B **109**, 8838 (2005).
[12] F. D. Bloss, *Optical Crystallography* (Mineralogical Soc. Am., Washington, D.C., 1999).
[13] M. Srinivasarao and J. O. Park, Polymer **42**, 9187 (2001).
[14] Y. Song, Ph.D. thesis, North Carolina State University, 1999.
[15] D. Axelrod, in *Methods In Cell Biology*, edited by D. L. Taylor and Y. L. Wang (Academic, San Diego, 1989), Vol. 30, Part B.
[16] A. Rapini and M. Papoular, J. Phys. (Paris), Colloq. **30**, C4-54 (1969).
[17] G. Barbero and L. R. Evangelista, *An Elementary Course on The Continuum Theory For Nematic Liquid Crystals* (World Scientific, Singapore, 2001).
[18] I. Dahl and A. D. Demeyere, Liq. Cryst. **18**, 683 (1995).
[19] A. Sugimura *et al.*, Phys. Rev. E **54**, 5217 (1996).